RAPID COMMUNICATION

The Structure of Isometric Capsids of Bacteriophage T4

Norman H. Olson,* Mari Gingery,† Frederick A. Eiserling,† and Timothy S. Baker*,1

*Department of Biological Sciences, Purdue University, West Lafayette, Indiana 47907-1392; and †Department of Microbiology and Molecular Genetics, University of California at Los Angeles, Los Angeles, California 90095-1489

The three-dimensional structure of DNA-filled, bacteriophage T4 isometric capsids has been determined by means of cryoelectron microscopy and image reconstruction techniques. The packing geometry of protein subunits on the capsid surface was confirmed to be that of the triangulation class $T = 13$. The reconstruction clearly shows pentamers, attributed to capsid protein gp24*, surrounded by hexamers of the major capsid protein, gp23*. Positions of the accessory proteins, Hoc and Soc, are also clearly delineated in the surface lattice. The Hoc protein is the most prominent surface feature and appears as an extended molecule with a rounded base from which a thin neck and a globular head protrude. One Hoc molecule associates with each hexamer. Nearly continuous "ridges" are formed at the periphery of the gp23* hexamers by an association of 12 Soc molecules; however, Soc is absent along the boundaries between the hexamers and the pentamers. The duplex DNA genome forms a highly condensed series of concentric layers, spaced about 2.36 nm apart, that follow the general contour of the inner wall of the protein capsid.   © 2001 Academic Press

Key Words: bacteriophage T4; cryoelectron microscopy; three-dimensional image reconstruction.

Introduction. Bacteriophage T4 is a large, double-stranded DNA virus (family *Myoviridae*) that infects *Escherichia coli.* Mature virions contain over 40 different polypeptides that form a prolate capsid, which encapsidates the ~170-kbp genome, and several other structural components, including a collar with whiskers, a neck, a tail with a contractile sheath, and a base plate with fibers (*14*).

The structure and morphogenesis of T4 capsids, and the closely related bacteriophage T2, have been extensively characterized using a variety of genetic and biochemical methods; however, previous structural analyses have primarily utilized negative-stain and metal-shadow electron microscopy (*6*). Many features of the T4 capsid structure were delineated from studies of a number of polymorphic variants of T4 and T2. Some of these include: (1) giants, which have abnormally long capsids that either occur naturally or can be produced from *in vitro* mutations and that sometimes have tails attached; (2) polyheads, which are long, open-ended tubes of gp23 often produced by mutations; (3) two-dimensional protein sheets of a proteolytic fragment of the main capsid protein, gp23; and (4) isometric and intermediate-length phage produced by "petite" mutations of gp23 (see (*6, 22*). These studies indicated that the mature T4 capsid is an elongated $T = 13l$ ($Q = 21$) icosahedron (*2, 6*). The mature virion shell is predicted to contain 160 hexamers of gp23* (48.7 kDa), 12 copies of gp20 (61 kDa) at the portal vertex, and 55 copies of gp24* (~44 kDa), arranged as 11 pentamers, at the remaining vertices. Post-assembly cleavage of gp23 and gp24 in proheads produces gp23* and gp24*, respectively, in mature virions (see (*6*)). Two accessory proteins, Hoc (40.4 kDa) and Soc (9.1 kDa) (highly-antigenic outer capsid protein and small outer capsid protein), which are not required for shell formation, decorate the capsid surface (*16, 17, 21*).

A detailed understanding of capsid morphogenesis requires structural information on the mature virion, on its components, and on assembly intermediates. Atomic-scale knowledge will ultimately be needed to identify specific interactions that occur among the various structural proteins throughout the process. In the interim, cryoelectron microscopy (cryoEM) and three-dimensional (3D) image reconstruction methods can provide a good source of reliable information that would otherwise be difficult to obtain through high-resolution techniques like X-ray crystallography. Because the techniques by which icosahedral particles can be reconstructed from cryoEM images are well established (*4*), DNA-filled, isometric capsids of T4 (hereafter, "isometrics") were selected for initial study. A 3D reconstruction of such capsids, calculated to a resolution limit of 15 Å and reported here, will serve as a starting point in the high-resolution determination of the mature, prolate structure. A recent
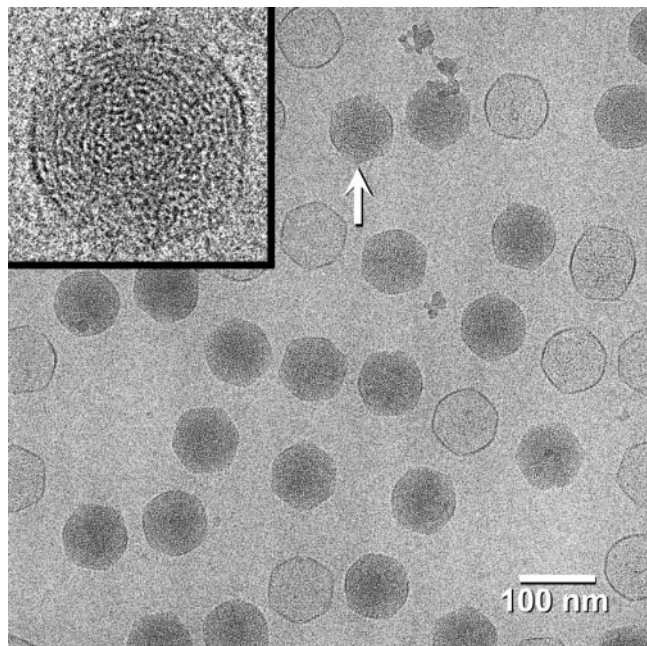

FIG. 1. CryoEM of bacteriophage T4 isometrics. Electron micrograph recorded at 1.86 μm underfocus of a field of DNA-filled and empty T4 isometric particles. Arrow indicates the filled particle shown in the inset which exhibits a "fingerprint" pattern consistent with the presence of highly condensed duplex DNA inside the capsid (see (6)).

paper (18) presents structural data on empty T4 isometric capsids that is consistent with our results.

Results. Frozen-hydrated, bacteriophage T4, 10*am*255/ 23*pt*2134-c mutants exhibited profiles in projection images characteristic of structures with an isometric morphology and which lacked the various appendages and tail found on wild-type virions (Fig. 1). Different orientations of the isometrics in the vitrified buffer yielded particle profiles ranging from nearly circular to hexagonal. Most isometrics contained densely packed DNA within their cores and the remaining particles appeared to be partially full or empty. Here we present results of a 3D reconstruction of just the DNA-filled particles (Figs. 2–4). As has been observed in a number of viruses (7, 8, 12, 13, 24), the compact DNA organization leads to characteristic "fingerprint" patterns in many of the isometric particles (Fig. 1, inset).

A 3D reconstruction was calculated from 862 images of T4 isometrics to 15 Å resolution (Fig. 2). The isometric T4 capsid has a rounded, hexagonal profile that arises from the 20 nearly planar, triangular, surface facets. The particle diameter varies from ~97.3 nm along the fivefold axes to ~87.9 nm along the threefold and twofold axes.

The organization of features on the surface of the isometric capsid is clearly consistent with an incomplete $T = 13$ skew, icosahedral lattice (11). In the absence of tilt experiments designed to determine the absolute hand of the reconstruction (e.g., (5)), we displayed our reconstruction as the $T = 13l$ enantiomer, consistent

with the hand observed in images of metal-shadowed phage surfaces (2).

The isometric capsid image shows 12 pentameric capsomeres at the vertices and 120 hexameric capsomeres (Fig. 3). Because the reconstruction was determined making use of 532-icosahedral symmetry, the visibility of the portal vertex, a dodecamer of gp20, was diminished owing to its being averaged with the 11 pentamers of gp24*. The hexameric capsomeres each contain 6 copies of gp23* (giving a total of 720 gp23* molecules; see (6)). They are located in two distinct sites in the icosahedron: 5 peripentonal hexamers lie adjacent to each of the 12 pentamers, and the remaining 60 (nonperipentonal) hexamers surround the 20 icosahedral, threefold axes of symmetry. The accessory protein, Soc, forms a nearly continuous, raised surface ridge (~8.5 × 2.7 × 1.4 nm) that encircles each of the nonperipentonal hexamers of gp23*, but encircles only the five sides of the peripentonal hexamers that are most distal to the pentamers (Figs. 2 and 3, top). Close inspection of surface views (Fig. 3, top) and radial-density projections (e.g., Fig. 3, bottom) reveals that while most gp23* molecules appear to be in contact with two Soc molecules, each of the 120 gp23* molecules closest to the pentamers contact only one Soc molecule (Fig. 5). Hence, the absence of Soc at hexamer–pentamer interfaces is what produces the incomplete ridge apparent about each of the peripentonal hexamers.

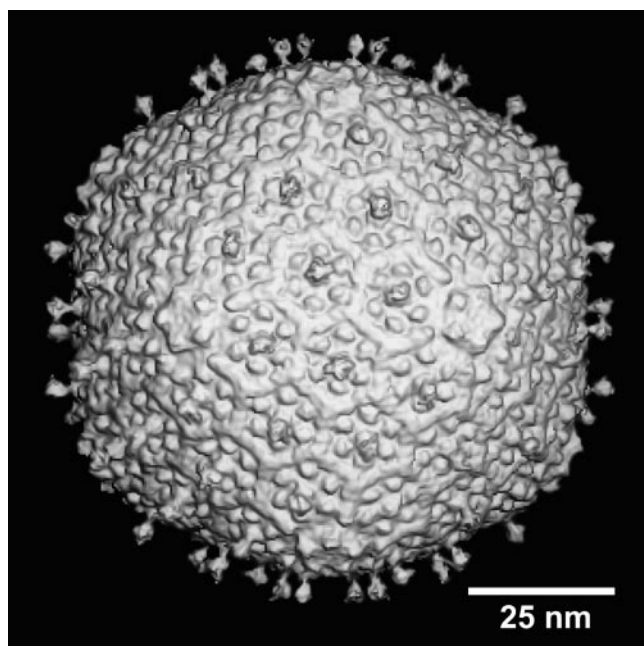The other accessory protein, Hoc, which is dispens-

FIG. 2. Shaded-surface rendering of the three-dimensional reconstruction of filled T4 isometrics. The view is along a twofold axis of the icosahedron. The prominent lollipop-shaped projections are Hoc molecules. A total of 120 such molecules extend outward from the center of each hexamer in the capsid.
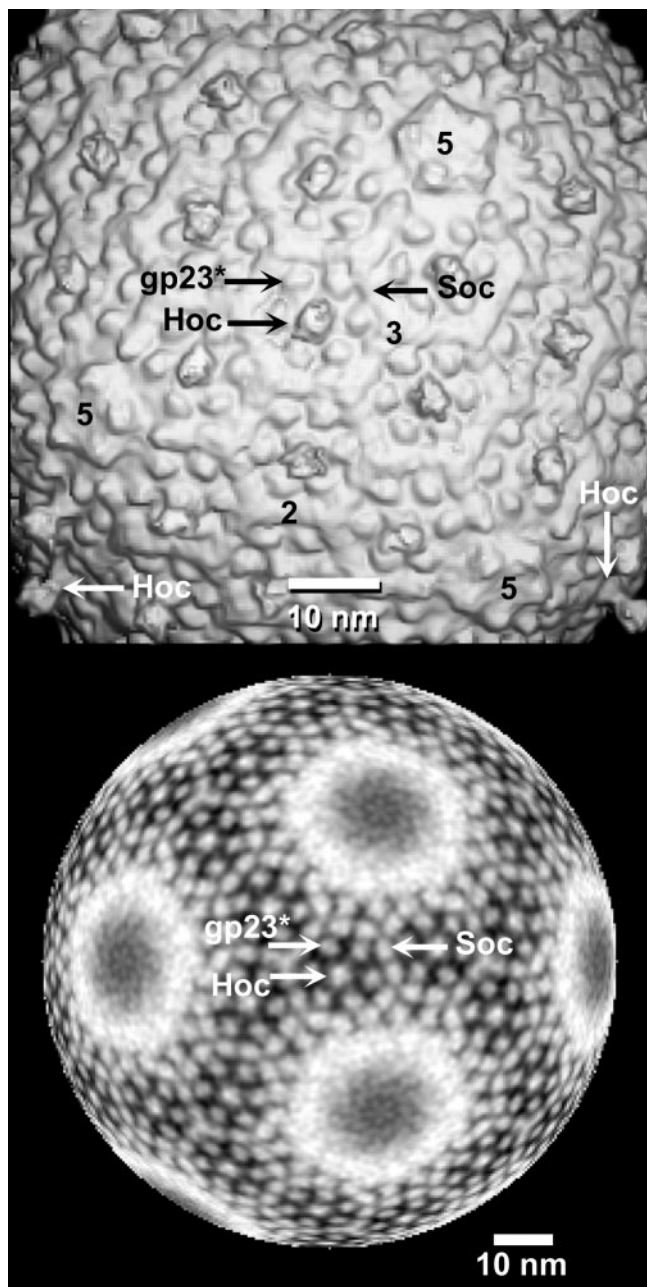
FIG. 3. Views, approximately along a quasi-sixfold axis, showing the organization of the T4 hexamers and pentamers. Top shows a close-up view of the T4 reconstruction with two-, three-, and fivefold axes identified for a single asymmetric unit (labeled 2, 3, and 5, respectively). Hexamers contain 6 copies of the main capsid protein, gp23*. Twelve molecules of Soc appear to form a nearly continuous ridge around each hexamer. A single Hoc molecule, with a thin stalk and a bulbous head, projects radially from the center of each hexamer. Pentamers of gp24* comprise the fivefold axes. The bottom shows the projected densities in the T4 reconstruction at a radius of ~43 nm, with contrast reversed to render high-density features in bright shades and low-density (e.g., solvent) as dark shades. At this radius, monomers of gp23*, Soc, and Hoc are distinguished.

rounded base (~1.9 nm high), a constricted neck region, and a globular head that is ~2.0 nm wide by ~2.4 nm high (Fig. 3, top). The shape of the globular head varies slightly between the two quasi-equivalent Hoc molecules. This is most likely a consequence of noise in the reconstruction and also flexibility in the neck which would permit the heads to adopt different positions relative to the capsid surface. The structure of Hoc is larger and extends farther than the one presented in a recent study of empty T4 isometric mutants (18).

According to theory (11), the number of capsomeres in a strict icosahedral capsid is given by the relation $10T + 2$, where T is the triangulation number. Hence, a strict $T = 13$ structure would consist of 132 capsomeres, of which 12 would be pentamers and the remaining 120 would be hexamers. The isometric T4 particles consist of 132 capsomeres with 120 hexamers of gp23*, 11 pentamers of gp24*, and 1 dodecamer of gp20 (see (6)). Hence, the T4 isometric capsid is not a strict $T = 13$ structure though the distribution of subunits follows the $T = 13$ pattern. In addition, each hexamer contains 1 Hoc molecule and the Soc molecules are distributed with a stoichiometry of 6 in each nonperipentonal and 4 in each peripentonal hexamer (Fig. 5). The overall stoichiometry of the primary structural proteins is thus: 720 copies of gp23*, 660 copies of Soc, 120 copies of Hoc, 55 copies of gp24*, and 12 copies of gp20. The morphologies and density levels of the gp23* and Soc molecules closest to the fivefold axes appear identical to the corresponding features in the nonperipentonal gp23* and Soc molecules. This suggests that the portal vertex (gp20 dodecamer) does not significantly alter the conformations of gp23* and Soc.

The inside core of the filled T4 exhibits a mass distribution that is a highly condensed set of concentric rings that follow the general outline of the inner surface of the capsid (Fig. 4). This distribution is consistent with an organized packing of the duplex DNA as is inferred by the fingerprint patterns in the images of many particles (Fig. 1, inset). This highly organized DNA packing persists for an annular region of at least 20-nm radius as can be seen in cross sections of the reconstruction (Fig. 4) and in a radial density profile (Fig. 4, inset). At least eight layers of DNA can be detected with an average interduplex spacing of ~2.36 nm, which is in close agreement with other independent measurements (see (6)).

Discussion. The reconstructed structure of DNA-filled, T4 isometric capsids has validated a number of assumptions concerning wild-type, prolate T4 capsids that have been made on the basis of information gathered from related structures. The current model for the organization of the T4 head has emerged from consideration of genetic, biochemical, and optical experiments performed with related or mutant phage structures (see (6)), along

able for capsid formation (16, 17), lies at the center of all 120 gp23* hexamers and extends ~5.0 nm above the capsid surface. It has a multidomain structure with a
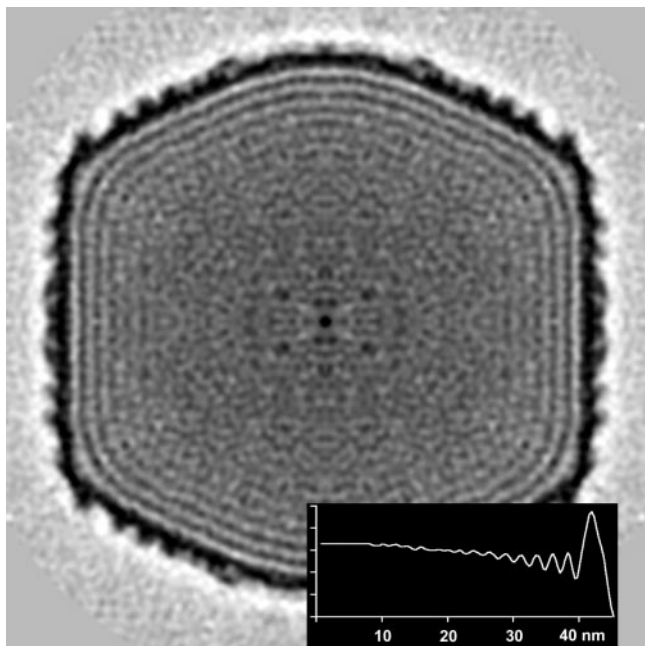
FIG. 4. Central section of the reconstructed T4 density map viewed along a twofold axis and rendered in normal contrast (high-density features appear dark). Concentric layers of alternating low and high density lie beneath the outer capsid shell. The dark layers are attributed to densely packed duplex DNA. The inset plots the spherically averaged density, computed from the three-dimensional reconstruction, as a function of radius. The highest density peak at the far right of the plot corresponds to the protein density in the outer capsid shell (~3.0 nm thick). At least eight progressively smaller peaks between radii of 38 and 22 nm arise from the condensed layers of duplex DNA. The spacing between successive rings is ~2.36 nm, which closely agrees with previous measurements of close packed DNA in bacteriophage T4 (see (6)).

with inferences based on icosahedral symmetry requirements (11). The $T = 13l$ packing geometry of the major capsid protein in T4 isometric capsids is identical to that found in T2 (9, 10) and T4 giant capsids (1), upon which the wild-type T4 model is based. This confirms the notion that all T4 head-length variants share a common geometrical architecture. It also adds credibility to proposed models of normal length capsids based on extrapolations from experiments with variants. The location and arrangement of the accessory proteins Hoc and Soc in isometrics matches previous reports (3, 28), and the vertices are clearly pentameric aggregates consistent with the presence of gp24*, as predicted (6).

The morphologies and distributions of Soc and Hoc in the capsid imply particular functional roles for each in phage viability, and hence may help explain the need for genetic investment in these nonessential proteins. The location of Soc molecules, bridging interhexamer interfaces, is consistent with their proposed role in reinforcing the junctions between adjacent gp23* hexamers. Soc stabilizes capsids against thermal denaturation (25), and exposure to detergent (26) or alkaline pH (17), suggesting that Soc may serve a role in preserving phage via-

bility in chemically hostile environments occupied by T4 hosts. The extended nature of Hoc is consistent with its identification as the most immunogenic capsid protein and a suggestion that it is well exposed (28). Though the separate domains of the Hoc molecule might suggest the presence of a fibrous (coiled-coil?) linker, examination of the amino acid sequence provides no obvious clues about the domain organization (unpublished observations). The location of Hoc implies that this molecule likely imparts little, if any, stability to the capsid. Indeed, the stability of capsids at alkaline pH is unaffected by the absence of Hoc (17), and Hoc binding only minimally affects the stability of the gp23* matrix against thermal denaturation (25). However, because Hoc has been reported to alter the affinity of some binding sites for Soc (3), Hoc may influence gp23* conformation and thus may exert an indirect affect on capsid stability. Although under standard laboratory conditions the function of Hoc is uncertain, its presence in the T4 genome implies that it provides some advantage for T4 survival, possibly in an environmental niche occupied by its natural bacterial host.
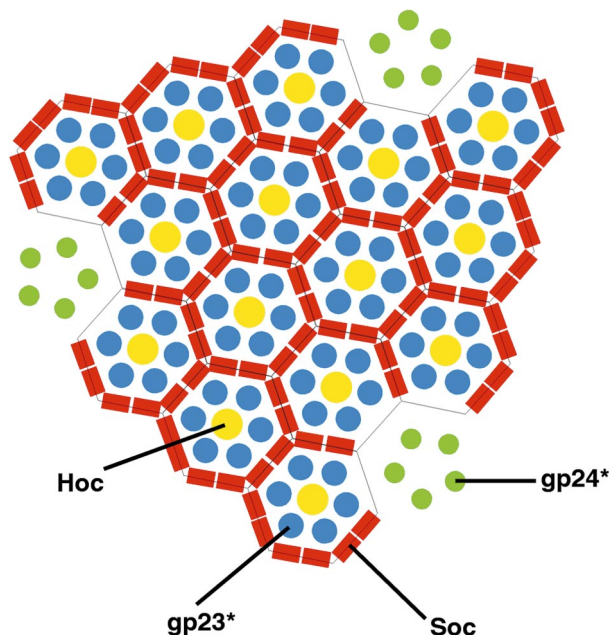

FIG. 5. Schematic representation of the distribution of capsid protein subunits within the $= 13l$ lattice (thin black lines) of the isometric T4 particle. The view direction is from outside the particle and along a threefold axis of symmetry. The region depicted includes three complete asymmetric units of the icosahedron (bounded by 3 gp24* pentamers) as well as small portions of adjacent asymmetric units for clarity. One Hoc molecule associates with each hexamer of gp23*. The 3 gp23* hexamers nearest the icosahedral threefold axis are each surrounded by a full complement of 12 Soc molecules. The peripentonal hexamers of gp23* (adjacent to the gp24* pentamers) are each surrounded by only 10 Soc molecules. This arrangement appears to be dictated by Soc interactions with adjacent gp23* subunits in neighboring hexamers. Soc molecules are absent wherever a gp24*–gp23* interface occurs, indicating that either gp24* or curvature in the surface lattice abrogates Soc binding.

A detailed examination of the T4 isometric reconstruction suggests some properties of Soc binding. Soc molecules have been proposed to form trimers (*3*), and the reconstruction shows Soc subunits in close contact at the trimeric sites of the surface lattice. However, the reconstruction also clearly shows that the 60 Soc molecules closest to the capsid vertices appear as monomers, implying that Soc only appears trimeric due to the arrangement of its binding sites. Early biochemical studies also indicated that Soc–gp23* interactions are favored over Soc–Soc interactions (*3*), and recent studies of Soc expressed in *E. coli* show it to be a monomer in solution (*18*). Thus, the binding of Soc may be dictated more by its interactions with neighboring gp23* molecules than by intersubunit interactions with other Soc molecules (Fig. 5).

The reconstruction gives clear evidence for the pentameric nature of gp24* at the vertices, in keeping with predictions based on symmetry constraints (*6*). The absence of Soc binding between gp23* and gp24* implies that each Soc requires interactions with two separate gp23* molecules, and therefore gp24* abrogates such interactions at the vertices. Whether this change in binding affinity is merely a result of steric hindrance or a result of some allosteric effect will require additional, especially higher resolution, analysis.

In light of the results that show a different arrangement of Soc molecules around peripentonal and nonperipentonal hexamers, the stoichiometry of the mature prolate phage differs from that of the predicted model (see (*6*)). Indeed, this study shows that the prolate capsid contains 160 hexamers of gp23* (960 molecules), 12 copies of gp20, 55 copies of gp24*, 160 copies of Hoc, but only 900 copies of Soc instead of the predicted 960.

Materials and Methods. Bacteria and phage. Phage was grown in *E. coli* B40su− cells. T4 mutant, 10*am*255/23*pt*2134-c, was used to produce isometric phage heads. This mutant is defective in tail assembly and produces a mixture of head sizes, including approximately 40% isometric heads (*23*).

Media and Buffers. M103 medium is M9 medium (*20*) + 1% Difco Casamino acids. CN (capsid, Na$^+$) buffer, a physiological glutamate-based buffer (*19*) to help stabilize encapsidated DNA, is 250 mM sodium glutamate, 10 mM putrescine, 5 mM MgSO$_4$, and 10 mM Tris, pH 7.5.

Preparation of Infected Cell Lysates for Purification of Isometric Heads. E. coli strain B40su− was grown at 37°C with vigorous aeration in M103 medium. Two hundred milliliters of culture was grown in a 500-ml Kluyver flask to a cell density of 4×10^8 cells/ml. The culture was then infected with T4 mutant 10*am*255/23*pt*2134-c at an input ratio of 5 phage per cell. After 9 min, the culture was superinfected with 5 phage per cell. At 120 min postinfection, cells were harvested by centrifugation. Infected cell pellets were resuspended in 10 ml CN buffer + 5 μg/ml DNase I and lysed by stirring with 0.5% CHCl$_3$ for 60 min. Cell debris was cleared by centrifugation at 9200 rpm for 15 min in a Sorvall SS-34 rotor.

Purification of Isometric Heads from 10am/23pt Lysates. Filaments of polymerized tail sheath protein (polysheath) were separated from capsids by PEG precipitation, taking advantage of the observation that filamentous structures precipitate at lower PEG concentrations than spherical ones (*27*). Cleared lysate was chilled to 4°C and held on ice with gentle stirring (all subsequent steps and solutions were at 4°C). Solid NaCl was added to increase the Na$^+$ concentration to 0.5 M. Polyethylene glycol (PEG-8000, as flakes) was added to a final concentration of 5% (w/v). The solution was stirred on ice for 60 min and held at 4°C overnight. Precipitated polysheath was removed by centrifugation at 9200 rpm for 15 min in an SS-34 rotor.

Supernatant from PEG precipitation was diluted with at least 2–3 vol CN buffer to reduce the PEG concentration and centrifuged at 25,000 rpm for 60 min in a SW41 rotor to concentrate phage heads. Pellets were covered with a small amount of CN buffer, held overnight at 4°C, and then gently resuspended.

Glycerol gradients (15–45%) were prepared in clear SW41 tubes by layering 5.8 ml 15% glycerol in CN buffer over 5.8 ml 45% glycerol/CN buffer. Gradients were formed by rotation in a Gradient Master (BioComp, New Brunswick, Canada) for 2 min at 25 rpm, at a tilt angle of 81.5°. A gradient was overlaid with 125 μl of highly concentrated PEG supernatant and centrifuged at 35,000 rpm for 60 min in a SW41 rotor.

DNA-filled capsids (heads) formed a wide band in the lower part of the gradient. The top and bottom portions of the broad band were recovered separately by syringe and needle through the side of the tube. Samples prepared for negative-stain electron microscopy contained predominately isometric heads in the top of the band and a mixture of mostly intermediate and normal prolate heads lower in the band.

DNA-containing heads from the top portion of the gradient band were diluted with sufficient CN buffer to fill a SW41 tube (about 15 vol). Heads were then concentrated by centrifugation at 25,000 rpm for 90 min in a SW41 rotor. The supernatant was discarded, and the tubes were carefully blotted dry. The pelleted heads were covered in a minimum volume of CN buffer, held overnight at 4°C, and then gently resuspended.

CryoEM and Image Reconstruction. CryoEM and image reconstruction procedures were performed essentially as described (*4, 15*). Images of the frozen-hydrated, DNA-filled and empty, isometric heads of T4 were recorded on Kodak SO-163 film in a Philips CM200 FEG microscope (FEI Company, Hillsboro, OR) at a nominal magnification of 38,000× and at an electron irradiation

level of $\sim$24 e^-/Å^2. Fourteen micrographs with defocus settings ranging from 1.8 to 2.8 μm underfocus were selected and digitized at 7-μm intervals with a Zeiss Phodis flatbed scanner (Carl Zeiss, Oberkochen, Germany). Pixels were binned to 14 μm, which represented 3.68 Å at the specimen level. A total of 1004 images of DNA-filled and partially filled ($\sim$2.5%) particles were extracted within circular windows from the scanned images. The initial origin and view orientation parameters for each virion image were determined by cross-correlation and "common lines" methods, respectively (see (*4*)). These parameters were then used to permit an initial, low-resolution, 3D reconstruction to be calculated and subsequently used as a starting model for the next step in the parameter refinement process. Refinement was carried out iteratively with use of the polar Fourier transform technique at progressively higher resolutions until no further improvement was noted as measured by several reliability criteria (see (*4*)). The final reconstruction, computed from 862 virion images, was corrected for both phase and amplitude effects of the contrast transfer function and was calculated to 15 Å resolution. Though the reconstruction was calculated to 15 Å, a more conservative estimate of the actual resolution limit achieved, as measured by various reliability criteria (see (*4*)), is $\sim$20 Å. These same criteria indicate that the noise limit of the data is reached at 15 Å. Adequate sampling of different particle orientations was ensured, as all values in the inverse eigenvalue spectrum of the reconstruction were <1.0. Since reconstructions computed from projection images emerge with arbitrary handedness, and we did not determine the absolute hand of the T4 isometric structure (e.g., (*5*)), the hand of the final reconstruction was set as the $T = 13$ *laevo* skew class. This is consistent with results obtained on metal-shadowed T2 virions (*9, 10*) and later confirmed for T4 (*2*).

ACKNOWLEDGMENTS

REFERENCES

1. Aebi, U., Bijlenga, R., van den Broek, J., van den Broek, R., Eiserling, F., Kellenberger, C., Kellenberger, E., Mesyanzhinov, V., Müller, L., Showe, M., Smith, R., and Steven, A. (1974). The transformation of τ particles into T4 heads. *J. Supramol. Struct.* **2**, 253–275.

2. Aebi, U., Bijlenga, R. K. L., ten Heggeler, B., Kistler, J., Steven, A. C., and Smith, P. R. (1976). Comparison of the structural and chemical composition of giant T-even phage heads. *J. Supramol. Struct.* **5**, 475–495.

3. Aebi, U., van Driel, R., Bijlenga, R. K. L., ten Heggeler, B., van den Broek, R., Steven, A. C., and Smith, P. R. (1977). Capsid fine structure of T-even bacteriophages. Binding and localization of two dispensable capsid proteins into the P23* surface lattice. *J. Mol. Biol.* **110**, 687–698.

4. Baker, T. S., Olson, N. H., and Fuller, S. D. (1999). Adding the third dimension to virus life cycles: Three-dimensional reconstruction of icosahedral viruses from cryo-electron micrographs. *Microbiol. Mol. Biol. Rev.* **63**, 862–922.

5. Belnap, D. M., Olson, N. H., and Baker, T. S. (1997). A method for establishing the handedness of biological macromolecules. *J. Struct. Biol.* **120**, 44–51.

6. Black, L. W., Showe, M. K., and Steven, A. C. (1994). Morphogenesis of the T4 head. *In* "Molecular Biology of Bacteriophage T4" (J. D. Karam, Ed.), pp. 218–258. Am. Soc. Microbiol., Washington, DC.

7. Booy, F. P., Newcomb, W. W., Trus, B. L., Brown, J. C., Baker, T. S., and Steven, A. C. (1991). Liquid-crystalline, phage-like packing of encapsidated DNA in herpes simplex virus. *Cell* **64**, 1007–1015.

8. Booy, F. P., Trus, B. L., Newcomb, W. W., Brown, J. C., Serwer, P., and Steven, A. C. (1992). Organization of dsDNA in icosahedral virus capsids. *In* "Proceedings of the 50th Annual Meeting of the Electron Microscopy Society of America" (G. W. Bailey, J. Bentley, and J. A. Small, Eds.), pp. 452–453. San Francisco Press, San Francisco.

9. Branton, D., and Klug, A. (1975). Capsid geometry of bacteriophage T2: A freeze–etching study. *J. Mol. Biol.* **92**, 559–565.

10. Branton, D., and Klug, A. (1975). Capsid geometry of bacteriophage T2: A freeze–etching study. *J. Mol. Biol.* **98**, 445.

11. Caspar, D. L. D., and Klug, A. (1962). Physical principles in the construction of regular viruses. *Cold Spring Harbor Symp. Quant. Biol.* **27**, 1–24.

12. Cerritelli, M. E., Cheng, N., Rosenberg, A. H., McPherson, C. E., Booy, F. P., and Steven, A. C. (1997). Encapsidated conformation of bacteriophage T7 DNA. *Cell* **91**, 271–280.

13. Earnshaw, W. C., King, J., Harrison, S. C., and Eiserling, F. A. (1978). The structural organization of DNA packaged within the heads of T4 wild-type, isometric and giant bacteriophages. *Cell* **14**, 559–568.

14. Eiserling, F. A., and Black, L. W. (1994). Pathways in T4 morphogenesis. *In* "Molecular Biology of Bacteriophage T4" (J. D. Karam, Ed.), pp. 209–212. Am. Soc. Microbiol., Washington, DC.

15. He, Y., Bowman, V. D., Mueller, S., Bator, C. M., Bella, J., Peng, X., Baker, T. S., Wimmer, E., Kuhn, R. J., and Rossmann, M. G. (2000). Interaction of the poliovirus receptor with poliovirus. *Proc. Natl. Acad. Sci. USA* **97**, 79–84.

16. Ishii, T., and Yanagida, M. (1975). Molecular organization of the shell of the T$_{even}$ bacteriophage head. *J. Mol. Biol.* **97**, 655–660.

17. Ishii, T., and Yanagida, M. (1977). The two dispensable structural proteins (*soc* and *hoc*) of the T4 phage capsid: Their purification and properties, isolation and characterization of the defective mutants, and their binding with the defective heads *in vitro*. *J. Mol. Biol.* **109**, 487–514.

18. Iwasaki, K., Trus, B. L., Wingfield, P. T., Cheng, N., Campusano, G., Rao, V. B., and Steven, A. C. (2000). Molecular architecture of bacteriophage T4 capsid: Vertex structure and bimodal binding of the stabilizing accessory protein, Soc. *Virology* **271**, 321–333.

19. Jardine, P. J., and Coombs, D. H. (1998). Capsid expansion follows the initiation of DNA packaging in bacteriophage T4. *J. Mol. Biol.* **284**, 661–672.

20. Kellenberger, E., and Sechaud, J. (1957). Electron microscopic studies of phage multiplication. II. Production of phage related structures during multiplication of phages T2 and T4. *Virology* **3**, 256–274.

21. Laemmli, U. K. (1970). Cleavage of structural proteins during the assembly of the head of bacteriophage T4. *Nature* **227**, 680–685.

22. Lane, T., and Eiserling, F. (1990). Genetic control of capsid length in bacteriophage T4. VII. A model of length regulation based on DNA size. *J. Struct. Biol.* **104**, 9–23.

23. Lane, T., Serwer, P., Hayes, S. J., and Eiserling, F. (1990). Quantized

viral DNA packaging revealed by rotating gel electrophoresis. *Virology* **174,** 472–478.

24. Lepault, J., Dubochet, J., Baschong, W., and Kellenberger, E. (1987). Organization of double-stranded DNA in bacteriophages: A study by cryo-electron microscopy of vitrified samples. *EMBO J.* **6,** 1507–1512.

25. Ross, P. D., Black, L. W., Bisher, M. E., and Steven, A. C. (1985). Assembly-dependent conformational changes in a viral capsid protein. Calorimetric comparison of successive conformational states of the gp23 surface lattice of bacteriophage T4. *J. Mol. Biol.* **183,** 353–364.

26. Steven, A. C., Couture, E., Aebi, U., and Showe, M. K. (1976). Structure of T4 polyheads. II. A pathway of polyhead transformations as a model for T4 capsid maturation. *J. Mol. Biol.* **106,** 187–221.

27. Vadja, B. P. (1978). Concentration and purification of viruses and bacteriophages with polyethylene glycol. *Folia Microbiol.* **23,** 88–96.

28. Yanagida, M. (1977). Molecular organization of the shell of T-even bacteriophage head. II. Arrangement of subunits in the head shells of giant phages. *J. Mol. Biol.* **109,** 515–537.